Acta Materialia 209 (2021) 116782

Contents lists available at ScienceDirect

Acta Materialia

journal homepage: www.elsevier.com/locate/actamat

Displacive or Order-Disorder Phase Transition? The H-bond Dynamics in Multicaloric Ammonium Sulfate

Leszek M. Malec, Mateusz Z. Brela*, Katarzyna M. Stadnicka*

Faculty of Chemistry, Jagiellonian University, Gronostajowa 2, 30-387 Kraków, Poland

ARTICLE INFO

Article history:
Received 16 June 2020
Revised 30 November 2020
Accepted 24 February 2021
Available online 28 February 2021

ABSTRACT

Recently, ferroic materials with giant caloric responses emerged as a possible environmental-friendly alternative for the currently used cooling devices. In our work, we have performed the Born-Oppenheimer molecular dynamics calculations for both para- and ferroelectric phases of multicaloric $(NH_4)_2SO_4$. The simulations were performed in the NVT ensemble with several conditions applied for three different supercell sizes. Time and space correlations between the ion motions were analyzed using various strategies to study the interaction changes along the obtained trajectories. The investigation of thermally induced evolution of complicated H-bond system in ammonium sulfate structure was performed using calculated power spectra. The results of simulations collated with the obtained X-ray diffraction data enabled us to describe the mechanism of $(NH_4)_2SO_4$ phase transition as the one of a mixed displacive and order-disorder nature. According to the origin of such structural transformation, the giant inverse barocaloric effect in ammonium sulfate is caused by the reverse H-bond system reorganization induced by hydrostatic pressure in the vicinity of the critical temperature. The spontaneous polarization observed in the ferroelectric phase is a secondary effect of symmetry change and it partially results from the disorder relaxation of both distorted NH_4^+ cations in low temperatures. The proposed investigation scheme should be useful in the studies of other ferrocaloric materials and H-bonded ferroelectrics.

1. Introduction

In the last few years, the giant caloric effects within ferroic materials were a subject of intense study in material science as the possible new environmental-friendly and efficient cooling devices [1-3]. Such refrigerators would give a possibility to replace the old ones, based on the vapor-compression method, which operates using fluids containing greenhouse gases. Additionally, the use of caloric effects enables the minimization of cooling devices [1]. To this day, the scientific efforts made to study caloric materials have resulted in several promising prototypes, mainly benefiting of magnetocaloric and electrocaloric effects [4-6]. Nevertheless, the applicability of magnetocaloric materials is limited by their high price and the necessity to generate strong magnetic fields (several teslas) [1,3]. The electrocaloric materials, despite the newest solutions leading to their much higher efficiency [7], are limited by the occurrence of the electrical breakdown. In contrast, the underlined problems in a great majority do not apply to barocaloric materials.

Recently, Lloveras et al. [8] found that relatively small changes in hydrostatic pressure (0.1 GPa at 219 K) induce a giant inverse barocaloric (BC) effect in the powdered ferroelectric ammonium sulfate (AS). The values of adiabatic temperature change $|T| = 8 \pm 1$ K, isothermal entropy change $|\Delta S| = 60 \pm 5$ $J \cdot K^{-1} \cdot kg^{-1}$, and $|\Delta T|/|\Delta p| = 80$ $K \cdot GPa^{-1}$ obtained for AS, are one of the largest ever known for BC materials. According to the additionally discovered electrocaloric (EC) effect in single-crystal plates [9], AS can be considered as not only ferrocaloric but also a multicaloric material. AS is an inexpensive, non-toxic compound commonly used as a fertilizer and a protein precipitant. It is a well-known H-bonded ferroelectric [10], crystallizing as big and durable crystals. The structural transformation of AS at $T_c = 223$ K results in the space group symmetry change from **Pnam** to polar **$Pna2_1$** [11,12]. In both, high-temperature paraelectric (PE) and low-temperature ferroelectric (FE) phases (Fig. 1), the unit cell contains four formula units, with one SO_4^{2-} and two symmetrically non-equivalent NH_4^+(I) and NH_4^+(II). As indicated in neutron diffraction studies, each of the ions in the PE phase has site symmetry **m**, which is lost during the phase transition (PT) [12].

Since the discovery of AS ferroelectricity in 1956, it has been studied using numerous experimental techniques to explain the

* Corresponding authors.
E-mail addresses: brela@chemia.uj.edu.pl (M.Z. Brela), stadnick@chemia.uj.edu.pl (K.M. Stadnicka).

https://doi.org/10.1016/j.actamat.2021.116782

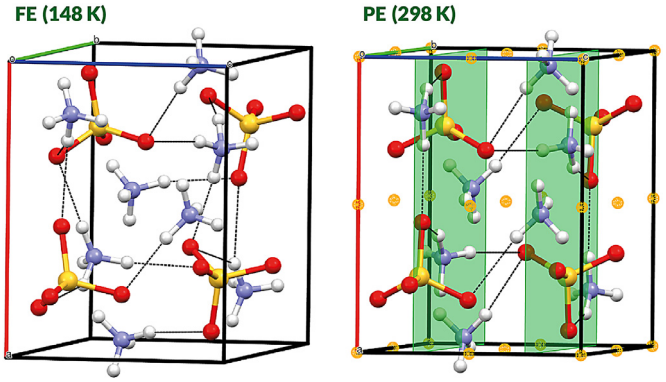

Fig. 1. AS unit cell in the FE (ferroelectric) and PE (paraelectric) phases. The strongest H-bonds in both phases are depicted by black dashed lines. Mirror planes and inversion centers, lost during the phase transition, are depicted by green surfaces and orange spheres, respectively.

mechanism of its PT. However, multiple spectroscopic investigations [13-25], X-ray and neutron scattering, and diffraction studies [12,26-30], as well as spontaneous polarization (P_s) measurements [31-33], did not result in one consistent theory of the PT. Instead, a few contradictory hypotheses describing the PT mechanism and thermodynamics were formulated [12,34-38]. Recently, we have joined the discussion of the structural PT in AS [39]. The obtained results enabled us to ascribe the origin of structural transformation to the thermally induced disruption of the lattice mode between SO_4^{2-} ions. The occurrence of P_s and its atypical T-dependence would be then the side effect of the H-bond system reorganization to the polar structure. However, the study of recently discovered caloric effects made us realize that further AS investigation is vastly needed. The nature of EC and inverse BC effects was ascribed to the order-disorder phase transition type [8,9]. This explanation, in contrast to the X-ray and neutron diffraction studies [12,27,39], assumes the disorder of all ions in the PE phase. Such an approach perfectly fits in the long-lasting dissonance between the descriptions of AS structure and PT based on the structural and spectroscopic data.

In this work, we will try to clarify this issue with a computational method – the Born-Oppenheimer Molecular Dynamics (BOMD) – that can produce data comparable with both structural and spectroscopic studies [40]. *Ab initio* BOMD simulations provide the 'on the flight' evaluation of electronic structure changes as well as atomic forces evolution via first-principles DFT computations at every time step. It is a perfect tool to characterize the dynamics of solid-state phases, including the temperature effects. BOMD features enable the studies of dynamical structural changes in the system as well as modeling of all kinds of the disorder [40-43]. The performed investigation is aimed to confront the structural X-ray diffraction data with the spectroscopic predictions of the disordered high-temperature AS phase. We used BOMD simulations of differently defined systems for a careful analysis of dynamics in both AS phases. Our studies will cast new light on the source of P_s and inverse barocaloric effect in AS.

2. Computational details

All BOMD calculations performed for AS were carried out using CP2K software [44,45]. Supercell approximation with periodic boundary conditions was considered in computations of both the PE and FE phases. The system size effect was discussed in SI, sections: S2 and S3. The first supercell type was obtained through the double replication of the unit cell along [100], [010], and [001] directions (**2×2×2**, 8 unit cells, 480 atoms). The second supercell type was prepared in the same manner but through the triple replication of the AS unit cell (**3×3×3**, 27 unit cells, 1620 atoms). The supercell examples were shown in Figs. S1-S2. The geometrical features of AS crystals were taken from our already reported structural data [39] and two additionally performed X-ray measurements at 298 and 148 K (see details in SI, Table S1). Thus, in our simulations the structural data at four temperatures were used, two close to T_c: 233 and 213 K, and two far from PT: 298 and 148 K. Supercell dimensions for all twelve systems used in calculations were listed in Table S2. Computations were performed for pre-optimized (MDaOPT) as well as for not optimized (MD) systems, giving a total of 24 different types of simulations. In each case, the symmetry **P1** was applied.

The GGA density functional BLYP (the Becke correlation functional [46] and the Lee, Yang, Parr electron exchange functional [47]) was used for the electron structure calculations. The D3-DFT Grimme correction for vdW forces was included [48]. The hybrid Gaussian and plane waves method was applied [49]. Mixed basis set with DZVP (for H, N, O atoms) and TZV2P (for S atoms) and plane waves was used. Cutoff kinetic energy was set to 250 Ry. For the core states description, Goedecker norm-conserving pseudo-potentials were used [50]. Further description considering the basis set choice was enclosed in SI (section S2). All simulations were performed in the canonical ensemble (NVT). The temperature control for the ionic degrees of freedom has been provided using Nosé-Hoover thermostat [51,52] with three chains and a 1000 fs time constant. Time step equal to 1 fs was used in all simulations. For each supercell 220,000 simulation steps were performed, giving the overall time of 220 ps, being adequate to simulate even the librational motions of heavy SO_4^{2-} ions. According to investigated E(t) dependencies, the last 200 ps of simulations were used in the further analysis. The trajectory was analyzed with the use of VMD software [53]. Power spectra were analyzed with the use of Fourier software [54].

3. Results and discussion

In the first step of the analysis, the potential energy and the performance of the thermostat were studied for all simulated systems (detailed description in section S3 in SI). As a result, the following interaction analysis was performed only for the simulations of 2×2×2 and 3×3×3 supercells. The 2×2×2 systems were justified by the analysis of potential energy and the temperature conservation along the trajectory. However, the insufficient replication of the studied system could be reflected by the improper characterization of interactions between neighboring molecules [42]. Therefore, further studies were performed also for 3×3×3 supercells for the inspection of the hydrogen bond network dynamics along the considered simulations.

3.1. Geometrical parameters in the simulated structures

To analyze the dynamics of AS in both phases, the quality of each structure replication was investigated. The study of geometrical parameters was based on the examination of distinct H-bond (HB) systems observed for each of four considered AS structures (at 148, 213, 233, and 298 K). The HB parameters are perfect indicators of ion relative positions and orientations. They also include information on the structure symmetry preservation. Hydrogen···acceptor distances (HA), donor–hydrogen···acceptor angles (DHA), and donor···acceptor distances (DA) were studied using several geometrical criteria. The parameters were calculated for each time step of the entire trajectory for all contacts of N–H···O type, which in the experimental crystal structure have HA $\leq$ 5.0 Å. Such threshold was chosen as it takes into account H···O distances for all H atoms of ammonium cation, which form HBs with

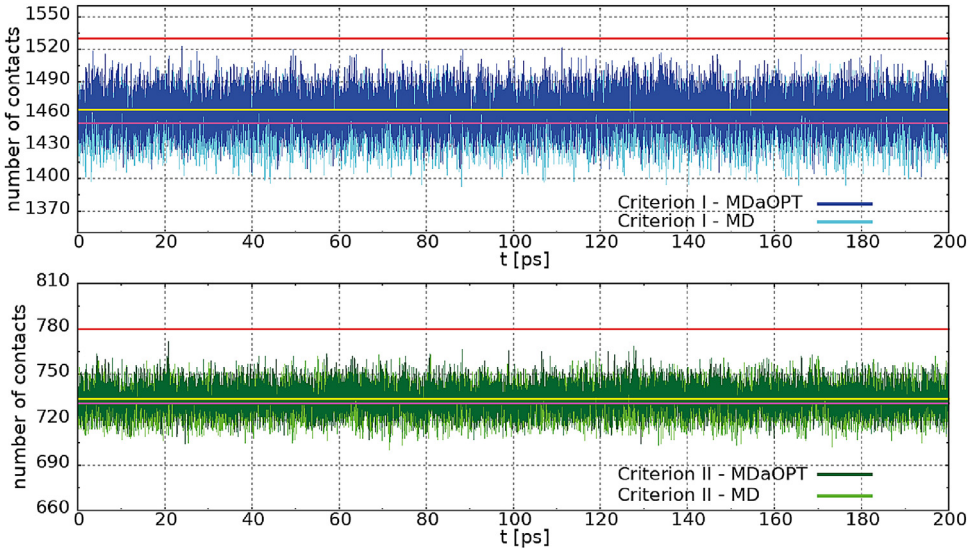

Fig. 2. Time dependence of replicated contact number in 3 × 3 × 3 systems at 148 K for Criterion I (up) and Criterion II (down). Red line – experimental value; yellow line – mean value for MDaOPT, magenta line – mean value for MD.

selected SO_4^{2-} anion. In this manner, not only all experimentally observed HBs were considered, but also those which could appear during the simulation as a result of the disorder.

The detailed description of the geometrical parameter analysis can be found in section S4 in SI. Regardless of the supercell size, MD simulations were found to fail in representing the experimental AS structure even at 148 K. In contrast, the MDaOPT computations replicated well almost all of HB parameters as well as the number of HBs at the lowest studied temperature. The obtained data indicate that in line with NMR [20,21] and IINS experiments [28-30], at higher temperatures (including 213 K in the FE phase), significant reorientations of both NH_4^+ cations are present in the AS structure. These movements remained invisible for neutron and X-ray diffraction experiments [12,26,27,39]. As a result, the performed analysis has shown that the study concerning only the time-averaged values of HB geometrical parameters is not sufficient to reproduce the full picture of intermolecular interaction dynamics in the AS phases. Therefore, in the next stage, methods concerning 'time step by time step' system evolution were used.

3.2. Time and space correlations in simulated systems

To analyze transformations appearing in the HB system at every time step, new geometrical criteria were introduced. These criteria, instead of the average values, concern only the temporary HA lengths and DHA angles. Criterion I assigns as an HB each N–H···O contact which, at a given moment of simulation, has HA length ≤ 2.9 Å and DHA ≥ 100°. Similarly to Criterion 1 in the mean value analysis (SI, section S4), Criterion I should enable the separation of all contact types which were proved to be intermolecular interactions at least in one of the AS phases [39]. A more restrictive Criterion II presupposes the HB geometrical criteria: HA length ≤ 2.5 Å and DHA ≥ 120° [55]. Using Criterion II, only the 'step by step' reproduction of interactions studied in section S4 was considered.

3.2.1. AS transient H-bond systems

The numbers of N–H···O contacts fulfilling either Criterion I or II were retrieved after every time step for each analyzed simulation. Each simulation of the low-temperature FE phase systematically indicates a lower number of contacts than expected from the crystal structures for both criteria (red lines in Fig. 2). The average number of replicated HBs is slightly higher for MDaOPT simulations (compare yellow and magenta lines in Fig. 2, Table S4). The same observations were made for minimal and maximal numbers of contacts (Tables S5-S7). Switching to the calculations of the PE phase, no changes were found for the above mentioned correlations, except for the larger differences between obtained and expected contact numbers for both criteria (Fig. S24). The analysis of the mean percent of replicated HBs as a function of simulation temperature gives similar values for both used criteria (Figs. S25-S26). For the FE phase, ca. 95% of the expected interactions were reproduced during the performed simulations, while for the PE phase, this value decreases to ca. 87%. The differences observed between the simulated phases as well as between obtained and expected contact numbers are mainly the results of Criteria definitions. N–H···O contacts with geometrical parameters close to the limiting values are almost entirely missed when the thermal vibrations are introduced. An example of such a phenomenon was recognized for 233 K simulations, where 116 (2×2×2) and 360 (3×3×3) contacts are very close to the limits of Criterion II (Fig. S26). Reduction of limiting HA length to ≤ 2.45 Å (Criterion II'), automatically gives the replication of the experimental system as good as for 298 K. It should be emphasized that approximately the same number of contacts fulfill Criterion I and II in both AS phases (Figs. 2 and S22, Table S4). The differences between simulated temperatures influence only the amplitudes of replicated contact numbers, which oscillate around the well-defined averages.

All so far obtained data, allow us to state that both 2×2×2 and 3×3×3 MDaOPT simulations replicate AS crystal structures and can be used to describe their properties and dynamics in both phases. The 3×3×3 simulations provide better statistics and a slightly better structure replication, therefore they were used in further analysis. It has to be emphasized that the MD computations do not replicate the experimental structures. In the thermostating process, the ions in MD supercells are significantly displaced or reoriented, causing the formation of H-bond systems different from those observed experimentally. A comparison of MD and MDaOPT calculations shows that the different systems of intermolecular interactions can be described with the same energy (Fig. S5).

3.2.2. Cation and anion dynamics

With the confidence of good AS structure replication, further studies concerned the ion dynamics. From the geometrical parameter analysis, it was found that both NH_4^+ cations significantly re-

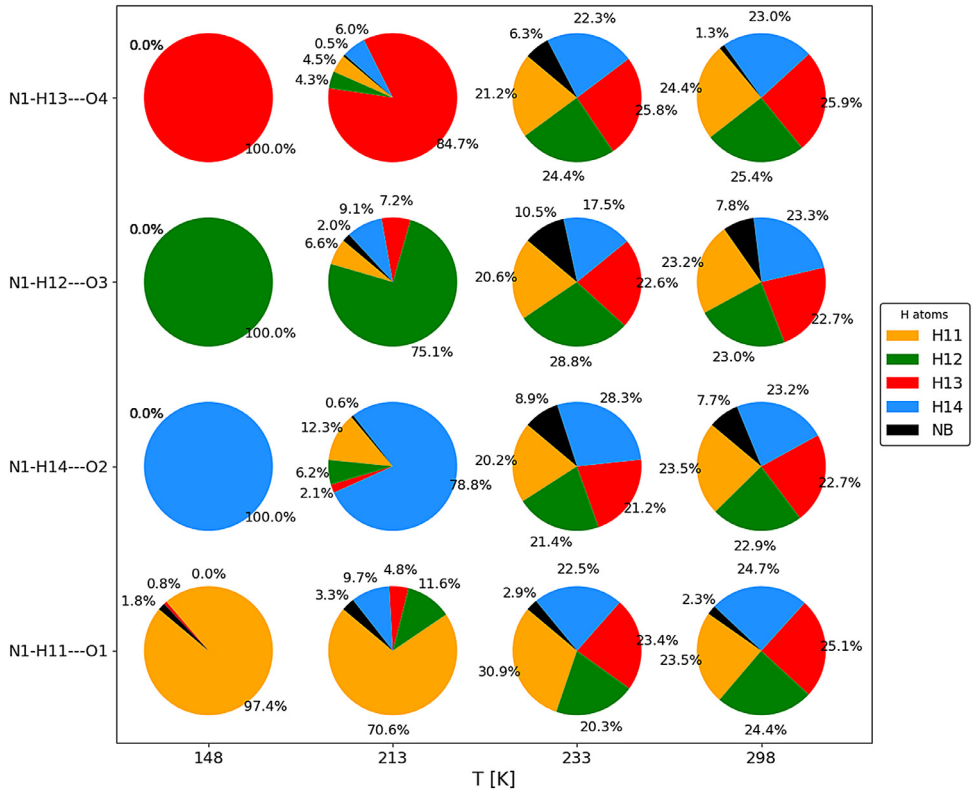

Fig. 3. Temperature dependence of contributions of specific H atoms of NH_4^+(I) to the strongest HBs in AS, according to Criterion I. NB (black color) represents a lack of H-bond formed between specified acceptor and NH_4^+(I).

orient in the PE phase. To study the influence of temperature on the changes in the relative orientations of cations and anions, one HB formed by each type of NH_4^+ cation was selected for each of the acceptors (2 HBs per acceptor). These eight X-ray determined HB types were chosen from the interactions that survive the PT and are possibly the strongest ones in both phases. Expecting some cation reorientations, the contributions of all H atoms to the selected HB types were analyzed. The contacts contributing to the specified HB type were verified along the entire trajectory according to Criterion I (HA length $\leq$ 2.9 Å and DHA $\geq$ 100°). If at a given moment, none of the H atoms fulfilled the above geometrical requirements, the contact was treated as "no bond" (NB). The obtained contributions were averaged over all H-bonds of a given type.

In Fig. 3 the results of such analysis for different simulation temperatures were compared for four selected HBs of NH_4^+(I). At 148 K, no reorientations of NH_4^+(I) ions were indicated in the studied time period. In line with the X-ray diffraction data, only one hydrogen is involved in each of the selected HB types. Moving closer to T_c, at 213 K, other H atoms of NH_4^+(I) than those determined by the structural analysis contribute to the studied H-bonds (Fig. 3). Their participation in the specific HB formation varies between 15 to 30%, being lower for stronger HBs and vice versa. The comparison of the DHA angles time evolution for one particular N1–H13···O4 indicated great similarities between motions of the NH_4^+(I) in both FE phase simulations (Figs. S27-S28). The amplitudes of DHA angles are larger at 213 K, however, no direct cation reorientation was observed. Here, it has to be recalled that the pie charts in Fig. 3 represent supercell averaged data. Therefore, in the case of N1–H13···O4 at 213 K, most of NH_4^+(I) ions bind to O4 only through H13 atom, while some of them experience at least one reorientation. The orientation change has to follow the rotation around one of the tetrahedron axes resulting in H atoms directly interchanging their positions. In this fashion, hydrogen atoms replace themselves at positions in crystal structure, which are well-defined by anion orientations. As a result, the persistence of interactions via HBs is provided (Fig. 3).

Just above T_c, in the PE phase at 233 K, the dynamics of NH_4^+(I) significantly changes. For each HB analyzed in Fig. 3, the contributions of H atoms evolve, heading towards equal distribution of all components. The largest contributions (ca. 30%) belong to H atoms which predominantly interact with selected acceptors in the low-temperature phase. Larger NB fragments, observed for all HBs except N1–H11···O1, are the result of weakening of these interactions in the PE phase [12,39]. The changes in the HB system between AS phases are caused by the difference in the dominating relative orientation of NH_4^+(I) and SO_4^{2-} (compare Figs. S28 and S29). At 233 K, the 35-40° librations of NH_4^+(I) out of the **ab** mirror plane were found. The hindered rotations cause the temporary change of NH_4^+(I) orientation to the one known from the FE phase. For the N1–H13···O4 example, such movements were observed at ca. 72nd and 183rd ps of the simulation (Fig. S29). The residence time [30] of the NH_4^+(I) in the FE orientation is very short, and did not exceed 2 ps in the studied case. The hindered rotations themselves occur in tens of femtoseconds. Similar randomization time [30] is characteristic for another type of movement recognized for NH_4^+(I) at 233 K, i.e. the tetrahedral reorientation described above for the 213 K simulation. The main difference observed for the PE phase is that the interchanging between H atom positions occurs for all NH_4^+(I) cations in the supercell. Such effect is caused by the significant reduction of the cation residence time in one orientation. For the N1–H13···O4 example, such time is equal to ca. 103 ps (between 7th and 110th ps in Fig. S29), however, for the precise estimation of NH_4^+(I) residence time at 233 K, a longer trajectory would be needed. Each tetrahedral reorientation indicated in Fig. S29 was caused by a different type of transformation. The

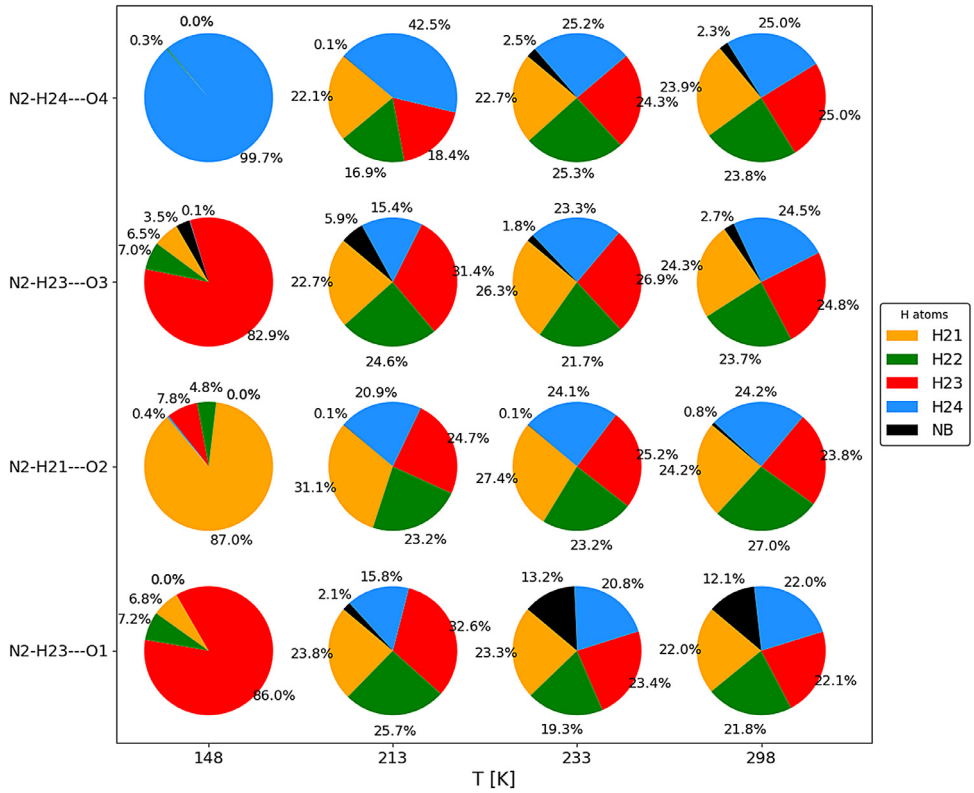

Fig. 4. Temperature dependence of the contributions of specific H atoms of NH_4^+(II) to the strongest HBs in AS according to Criterion I. NB (black color) represents a lack of H-bond formed between specified acceptor and NH_4^+(II).

first one, at 7th ps, would be generated as the reflection across the mirror plane bisecting H13−N1−H12 valence angle. As such transformation is physically impossible, it was in fact a combination of two rotations. First, NH_4^+(I) rotates about a 4 rotoinversion axis placed along the bisector of the H13−N1−H12 angle. Subsequently, it rotates about a 2-fold axis placed along the bisector of the H13−N1−H14 angle. The latter reorientation, at 110th ps, was performed through a rotation of NH_4^+(I) about a 3-fold axis placed along the N1−H13 bond.

At 298 K, the picture of NH_4^+(I) dynamics further complicates because of a frequent simultaneous occurrence of tetrahedral reorientations and the hindered rotations out of the **ab** plane (Fig. S30). Such interference is induced by a striking reduction of residence time for the tetrahedral interchange of H atoms. For the studied N1−H13···O4, the residence time did not exceed 20 ps. As a result, the almost equal distribution of all H atoms between the analyzed H-bonds was indicated (Fig. 3). At 298 K, the change in the occurrence frequency of NH_4^+(I) hindered rotations was also observed. The librations between the two orientations are separated with intervals not longer than 10 ps. The PE orientation, observed mainly at 233 K, is characterized by average DHA angles 120°, 100°, 40°, and 40°. It is dynamically replaced by the FE orientation with 170°, 60°, 60°, and 50° average DHA angles (Fig. S30). In contrast to 233 K simulation, at 298 K, the NH_4^+(I) preserves the FE orientation for periods lasting up to ca. 10 ps. As a consequence, the NH_4^+(I) distribution between FE and PE orientations is approximately equal at 298 K. The same degree of stabilization observed for both orientations is caused by larger librations of SO_4^{2-} anions in the PE phase.

The space averaged picture of NH_4^+(II) dynamics at 298 K (Fig. 4) is almost identical to the one observed for the NH_4^+(I). Each H-atom of the NH_4^+(II) is equally involved in all four studied HBs. However, the direct analysis of DHA angles time evolution for one exemplary N2−H24···O4 has indicated significant differences between both NH_4^+ reorientations (Fig. S31). As for the NH_4^+(I), for the NH_4^+(II), two main motion types were characterized: the hindered rotations between FE and PE orientations and the tetrahedral reorientations. The main differences observed for the NH_4^+(II) cations are the lower residence time of both above mentioned movements. The hindered rotations were split with intervals shorter than 4 ps, while the reorientations were separated with periods not longer than 14 ps. The short residence time of both motions caused their frequent simultaneous occurrence, which did not allow us to describe the individual transformations between different NH_4^+(II) orientations (Fig. S31).

At 233 K, some sort of stabilization was indicated in NH_4^+(II) dynamics. Although the supercell averaged description of the NH_4^+(II) tends to be constant in the PE phase (Fig. 4), notable changes were found through the analysis of individual HBs. At 233 K, the observed residence time between tetrahedral reorientations elongated even up to 37 ps (Fig. S32). Such value remains much shorter than the one found for the NH_4^+(I) at the same temperature (ca. 100 ps). In the N2−H24···O4 example, the tetrahedral reorientations were accomplished in two ways. Either by the rotation about a 3-fold axis placed along one of the N2−H bonds or through the rotation about a 2-fold axis placed along the bisector of one of the H−N2−H valence angle. In contrast to NH_4^+(I), at 233 K, NH_4^+(II) frequently twists between the FE and PE orientations. The overall residence time of the NH_4^+(II) in the FE orientation significantly decreased in comparison to the one observed at 298 K. However, while approaching the T_c from the above (in a cooling manner), the NH_4^+(II) remains much more thermally disrupted than the NH_4^+(I) (compare Figs. S32 and S29).

Such observation is valid also for the cation dynamics comparison in the 213 K simulation. The analysis of H atom contributions for the NH_4^+(II) just below T_c has indicated the persistence of the

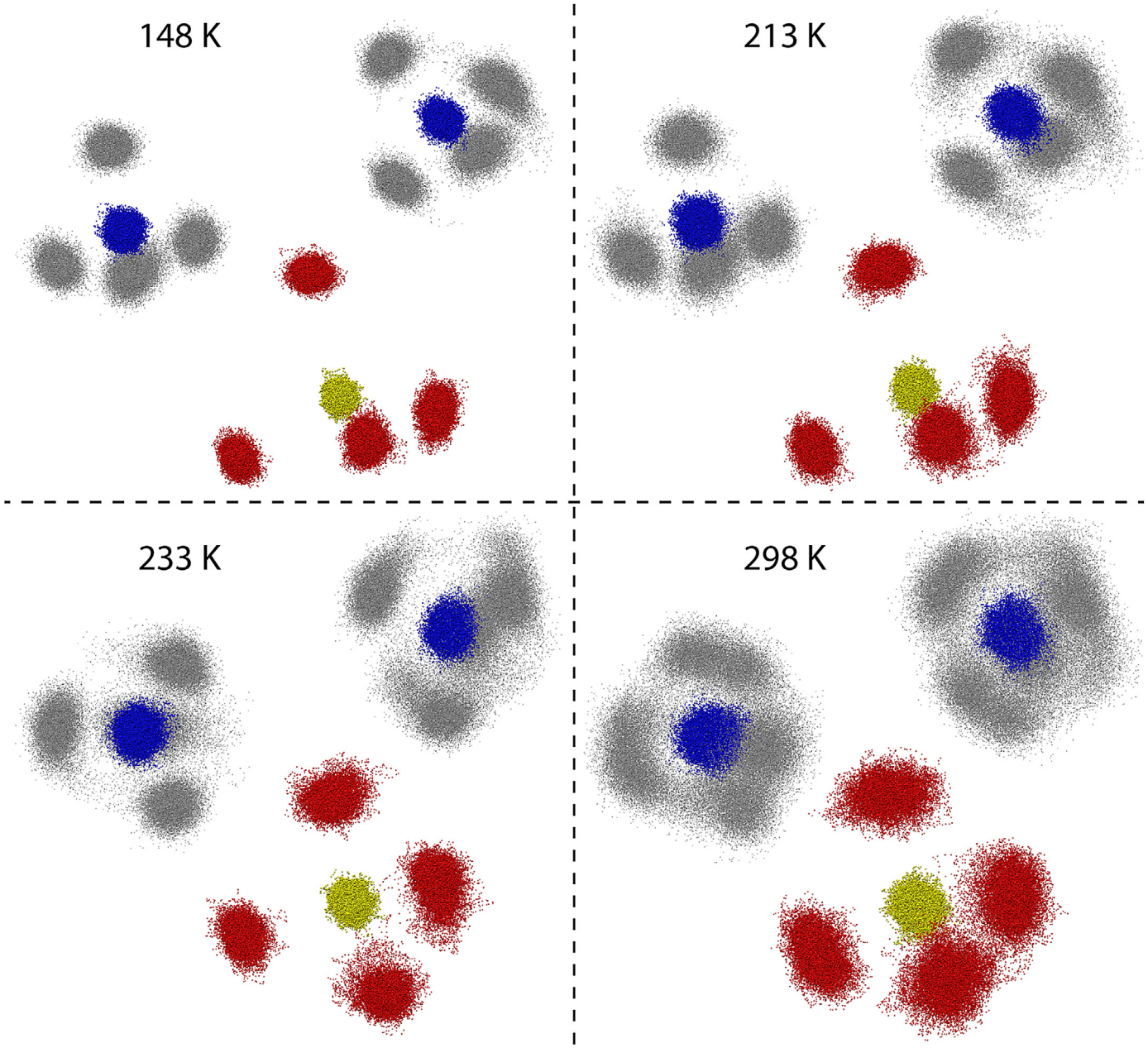

Fig. 5. Temperature dependence of spatial distributions of atoms in the AS asymmetric unit from 3×3×3 MDaOPT simulations (NH_4^+(I) - left, NH_4^+(II) - right). Each dot represents an atom position during simulation.

tetrahedral reorientations observed in the PE phase (Fig. 4). Each hydrogen was found to contribute to the formation of all studied HBs. The residence time between the reorientations significantly increased with respect to the one observed at 233 K (Figs. S32 and S33). Various independent reorientations of cations in the supercell resulted in the averaged picture resembling those indicated at higher temperatures (Fig. 4). In contrast to the PE phase, at 213 K, the contributions are not evenly distributed and vary depending on the HB type. The H atoms which predominantly interact with selected acceptors are the ones detected in the structural studies of the FE phase. It is especially pronounced for the strongest HB formed by the NH_4^+(II), i.e. N2−H24···O4. The major contribution of H24 to this HB, together with its smaller impact on the other HBs, indicate the emergence of the main rotation axis along the N2−H24 bond. It should be noted that, at 213 K, the NH_4^+(II) orientation was additionally disrupted by the hindered rotations between the FE and PE orientations. Such twists were not observed for the NH_4^+(I) in the FE phase. Switching between the orientations was irregular and occurred multiple times during the entire trajectory (Fig. S33). Inferring from the big differences between residence time in both orientations, it is clear that the PE orientation is much less stable at 213 K than above T_C.

Moving to 148 K simulation, further stabilization of the NH_4^+(II) in the FE orientation was indicated (Fig. S34). The hindered rotations nearly disappear, however, the observed DHA angle amplitudes remain higher than those found for the NH_4^+(I). Even at such low temperatures, the interchange between H atom positions was detected for the NH_4^+(II). In contrast to 213 K simulation, the tetrahedral reorientations are realized only through the rotation about a 3-fold axis along N2−H24. Thus the strongest HB in the FE phase is stable, while multiple H atoms are contributing to weaker HBs (Fig. 4). The residence time between the re-

orientations significantly increases comparing with those in the simulations at higher temperatures. Therefore, along the studied trajectory, the tetrahedral reorientations occurred only for several NH_4^+(II) in the entire supercell.

To clarify and sum up the ion dynamics description, the spatial distribution of atoms from the AS asymmetric unit were compared for the simulations at all studied temperatures (Fig. 5). The data were visualized for asymmetric units placed in the closest vicinity of the geometrical center of 3×3×3 systems. In line with the preceding structural analysis, SO_4^{2-} ions are not disordered in the high-temperature phase. The larger ellipsoidal-shaped distributions of O atoms result from the greater SO_4^{2-} librations in the PE phase. As expected, this effect diminishes in lower temperatures, despite the persistence of NH_4^+(I) and NH_4^+(II) tetrahedral reorientations.

At 298 K, H atom distributions of both cations have a form of very elongated ellipsoids, which consist of two maxima connected to the PE and FE orientations, respectively (Fig. 5). Blurred regions between the ellipsoids result from the tetrahedral reorientations between H atom positions. The observed distributions enable us to classify cation motions in the high-temperature phase as a dynamic disorder [56]. At 233 K, the PE orientation dominates for both cations but seems to be not stable with further temperature decrease. Below T_c, NH_4^+(I) cations immediately stabilize in the FE orientation. The residence time between tetrahedral reorientations rapidly elongates, and at 213 K, surpasses the simulation length. In contrast, the NH_4^+(II) reorientations were clearly indicated in both simulations of the FE phase. Although the PE orientation is significantly less stable below T_c, the NH_4^+(II) hindered rotations do not freeze in the FE phase (Fig. 5). Therefore, for one cation type, the so-called "ferroelectric mode" [20,21] remains active even below the T_c.

3.3. Power spectra

Performed BOMD simulations allowed us to calculate the power spectra for AS crystal at the four simulated temperatures using the Fourier transform of atom position autocorrelation functions (Fig. S35). Such an approach enables the analysis of all active modes in one spectrum [57]. Each calculated spectrum contains bands expected for internal modes of the distorted tetrahedral ions [58]. The modes were assigned using multiple experimental data [13,14,59]. Broad band between 2750-3750 cm^{-1} emerges as the superposition of symmetric (ν_1) and asymmetric (ν_3) stretching modes of two NH_4^+ types (Fig. 6). At 298 K, the broad asymmetric band has one maximum at ca. 3350 cm^{-1}. At lower temperatures, three maxima at 3427 cm^{-1}, 3323 cm^{-1}, 3151 cm^{-1} gain on intensity with temperature (T) decrease. The red-shift expected for high-temperature spectra was observed for 1630-1750 cm^{-1} band of NH_4^+ scissoring modes (ν_2, Fig. S36). Another two close-placed bands between 800-1180 cm^{-1} result from ν_1 and ν_3 modes of SO_4^{2-} anion (Fig. S37). The ν_2 and ν_4 modes of SO_4^{2-} were assigned to bands with peaks at 583 cm^{-1} and 434 cm^{-1}, respectively.

To further analyze the generated spectra, each band was decomposed into the increments of individual ion types (NH_4^+(I), NH_4^+(II), SO_4^{2-}). For the N–H stretching region, such a procedure corroborated significant differences in H-bonding and dynamics of NH_4^+(I) and NH_4^+(II) (Fig. 6). At 298 K, the components of both NH_4^+ have maxima shifted towards higher wavenumbers with broad shoulders at ca. 3200 cm^{-1}. In line with the ion dynamic analysis, NH_4^+(I) is exposed to more pronounced changes with the temperature decrease. Two equally intense maxima are well separated already at 233 K, i.e. before the PT. In the FE phase, the peak at lower frequency intensifies with T decrease, while the second maximum gets narrower and shifts towards lower wavenumbers.

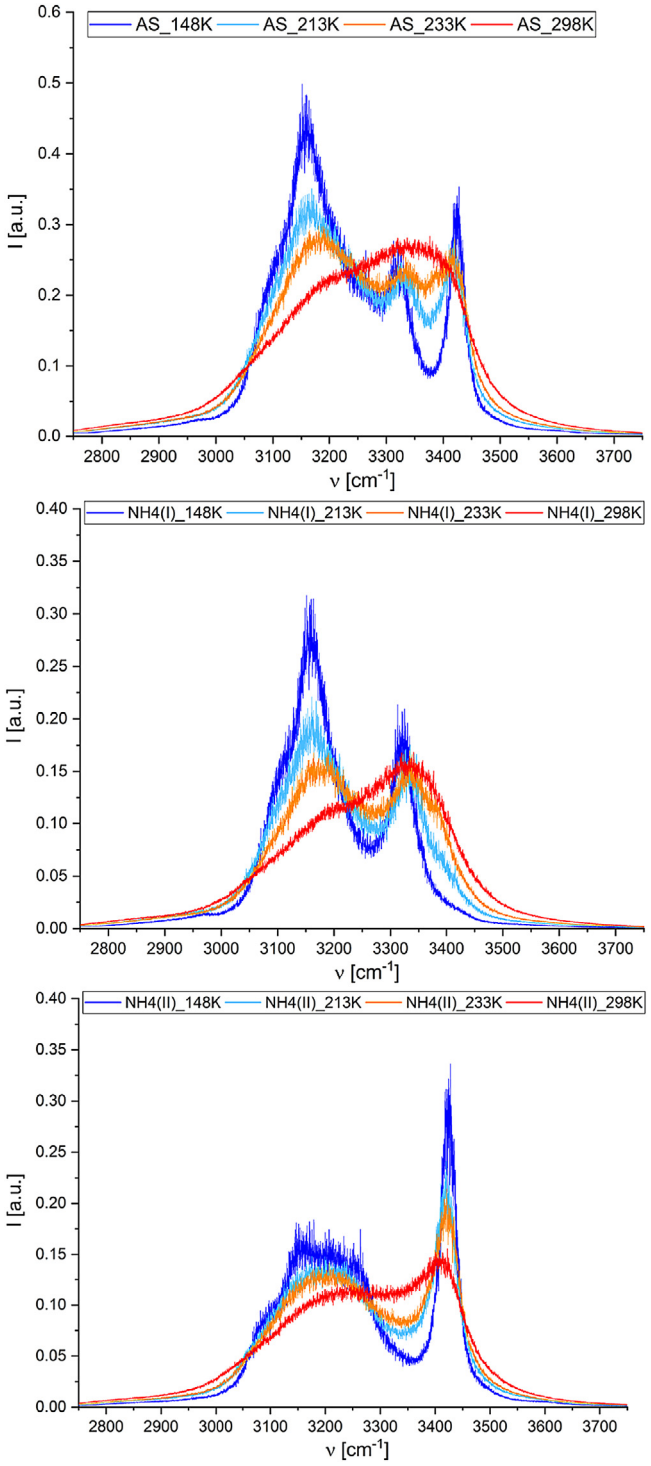

Fig. 6. Comparison of high-frequency region of AS power spectra for all used simulation temperatures (top). Decomposition of full power spectra into the separate contributions of NH_4^+(I) and NH_4^+(II) (middle and bottom respectively).

Within two simulations in the vicinity of PT, the high-frequency bands of the NH_4^+(II) are almost identical (Fig. 6, bottom). The narrow peak at 3425 cm^{-1} intensifies and shifts towards higher frequencies with the T decrease. The broad peak at ca. 3200 cm^{-1} remains complex at 148 K, however, some irregular intensity increase was observed at lower wavenumbers. Further decomposition of the spectra into the contributions of individual N–H bonds has shown that such an effect is a result of the stabilization of

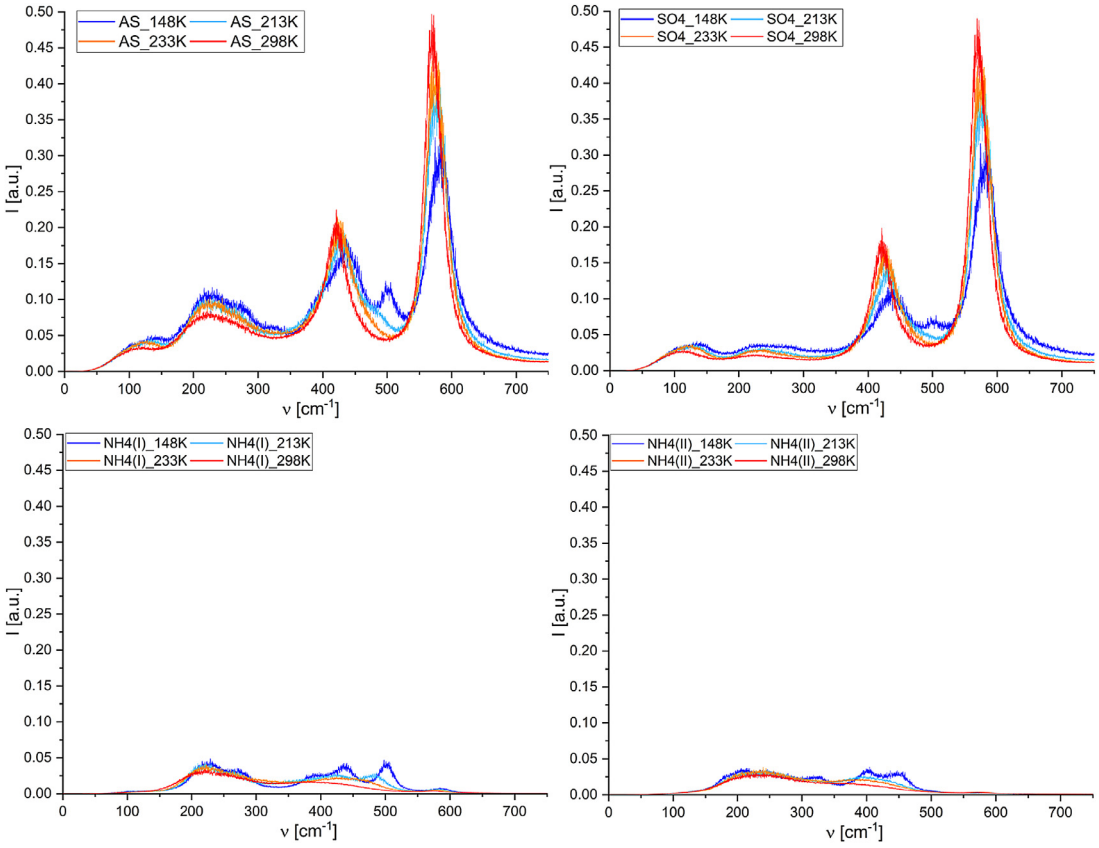

Fig. 7. Low-frequency region of AS power spectra for all used simulation temperatures (top left). Decomposition of full power spectra into the separate contributions of SO_4^{2-}, NH_4^+(I), and NH_4^+(II) (top right, bottom left, and bottom right, respectively).

the H24 atom position via strong HBs (Fig. S36). It has to be emphasized that the method used for spectra generation cannot fully separate the individual N–H bond oscillations from the other vibrations of the same type. The impacts of other N–H stretching modes are transferred through the N atom to each component. Therefore, even at 148 K, two peaks are observed at each spectrum: the main one and the secondary one with lower intensity (Fig. S36). At higher temperatures, those additional peaks intensify as a result of interchange between H atom positions within the tetrahedral reorientations. The existence of H atom interchange in the PE phase is also indicated by the identical band components observed for all the N–H bonds of the selected cation type (Figs. S39-S40). This effect is still noticeable for the NH_4^+(II) in the FE phase at 213 K. In the case of the NH_4^+(I), the reorientations become rare after the PT, and as a consequence, the band components of symmetrically nonequivalent N–H bonds differ from each other. The position less stabilized by HBs becomes mainly occupied by the H11 atom. The partial stabilization of H atoms of NH_4^+(II) at positions known from the structural analysis was indicated only for 148 K simulation (Figs. S38 and S40). The hydrogen position in a very weak N2–H···O2 becomes mainly occupied by the H22 atom. The main peak of the N2–H24 component is significantly shifted towards lower frequencies, while the secondary one at 3427 cm^{-1} becomes less intensive when compared to other bond contributions. These observations are in line with the emergence of NH_4^+(II) main rotation axis along N2–H24, postulated in the ion dynamic analysis.

To complete the AS power spectra analysis, the anion and lattice modes were carefully studied. Moving through the transition point, no distinctive changes were indicated for individual contributions of S–O bonds. In contrast, 10 K above the PT, the S–O stretching region substantially changes for the S1–O1 component (Figs. S41-S42). In comparison to the same band at 298 K, the intense maximum occurs at ca. 1060 cm^{-1}. With further T decrease, the peak in the S1–O1 component shifts towards higher frequencies. From previous studies, it is known that the O1 atom is the less H-bond stabilized acceptor in both AS phases [39].

In agreement with the experimental studies [13,14,25], no mode softening was observed in the 100–4000 cm^{-1} spectral range (Fig. 7). From the calculated low-frequency bands, only the peak at ca. 115 cm^{-1} is a result of one ion type vibrations i.e. SO_4^{2-} translations [59]. Bands observed between 150-350 cm^{-1} arise from lattice modes involving both cation translations and anion librations (Fig. S43). Moreover, with temperature decrease, the coupling between v_2 SO_4^{2-} and NH_4^+(I) lattice modes was indicated. The additional band for the NH_4^+(I) starts to emerge at 233 K. With further cooling, the band gains on intensity and shifts towards higher frequencies till 498 cm^{-1} at 148 K. The engagement of the SO_4^{2-} into this new mode is signalized in the FE phase. All symmetrically nonequivalent S–O oscillators seem to be involved in the vibration characterized by broader signals for S1–O2 and S1–O4 bonds and narrower peaks for S1–O1 and S1–O3 (Fig. S44). Much more intense maxima for N1–H13 and N1–H14, obtained after NH_4^+(I) band decomposition, suggest the librational nature of the lattice mode (Fig. S45). NH_4^+(II) is not involved in this type of vibration (Fig. 7, Fig. S43). The only changes in its lattice modes were indicated at the lowest simulated temperature.

3.4. Phase transition mechanism and the origin of AS properties

Recent works on the electrocaloric and inverse barocaloric (BC) effects considered the AS phase transition as the ordering of the

entire asymmetric unit in the process of two-step structural transformation [8,9]. Such an approach has originated from the multiple experimental investigations [14,17,20-26,29-33]. Despite similar observations, various interpretations were formulated classifying AS either as a pseudo-proper ferroelectric or as a ferrielectric material [17,34,36,38]. Most of the discrepancies between these hypotheses can be verified by our investigation.

Above the PT, in the PE phase, the AS unit cell volume is continuously reduced with decreasing T [8,39]. Simultaneously with the unit cell contraction, crucial changes develop in the ion dynamics. With crystal cooling from RT to the vicinity of T_c, the SO_4^{2-} librations are significantly suppressed, despite the persistence of NH_4^+(I) and NH_4^+(II) tetrahedral reorientations and hindered rotations. For both cations, the residence time for both motions increase. However, the striking elongation of these time is observed only for NH_4^+(I) motions. The critical slowing down of the NH_4^+(I) hindered rotations ("ferroelectric mode") is induced by the SO_4^{2-} orientation change signalized in the SO_4^{2-} asymmetric stretching band. The O1 atom is displaced into the less HB stabilized position and the HB chain co-created by bifurcated interactions in the **bc** plane is disrupted (Fig. S46). The indicated anion reorientation was earlier described as the precession about an axis placed close to the S1−O2 direction, which breaks the PE symmetry [39]. The O1 main peak in the ν_3 band significantly shifts towards higher frequencies and a small frequency increase is observed for the O3 and O4 components of the same band (Figs. S41-S42). As a result of anion precession, the coupling between NH_4^+(I) librational modes and SO_4^{2-} ν_2 scissoring modes arises (Fig. 7, Fig. S43) and the relaxation of NH_4^+(I) hindered rotations proceeds. In line with the observed picosecond-long residence time, such softening was indicated in the submillimeter spectral region [25]. The energy transfer between the modes of coupled ions occurs mainly through N1−H13···O4 and N1−H14···O2 interactions (Figs. S44-S45). The new HB system formation induces greater NH_4^+(I) distortion resulting from the larger diversity in the H-bond stabilization of the spatial positions of individual H-atoms (Figs. S38-S39). Below T_c, at 213 K, the NH_4^+(II) hindered rotations are still not totally suppressed. The long residence time, observed for that motion, suggest a quite immediate completion of its relaxation process with further cooling. In agreement with the experimental results [20,21,29,30], the tetrahedral reorientations of both cations do not fade away during the PT. In the case of the NH_4^+(II), the relaxation process of this motion exceeds the studied temperature range.

The anion orientation change occurring in the first step of the PT significantly influences the unit cell volume dimensions. The H-bond system reorganization, enforced by the SO_4^{2-} precession, is accompanied by a step-like contraction of **b** and **c** lattice vectors [39,60]. While the parameters in the **bc** plane decrease, the steep increase in length is observed for **a**. Such expansion is caused by the alignment of the S1−O1 bond along [001] accompanied by the formation of a new moderate N1−H12···O3. These structural changes are further stabilized after PE symmetry breakdown at T_c. The above analysis indicates that the inverse BC effect originates in simultaneous compression of the lengths of the lattice vectors, which enforces the inverse anion reorientation and therefore reverses the H-bond reorganization. The heat has to be transferred into the crystal to stabilize the HB system in the PE phase structure arrangement by the appropriate librations and NH_4^+ hindered rotations.

Finally, the source of the spontaneous polarization, inseparably connected to the PT, should be discussed. The atypical T dependence of P_s in AS crystals [31,32] was ascribed to the competing contributions of all distorted ions [15,16] or exclusively to cations [24]. Subsequent theories considered also the impact of the so-called 'lattice polarization', which would arise from the shifts of both cations out of the **ab** plane in the FE phase [17]. However, according to our results, the crucial information seems to be hidden in the P_s study of the mixed $(NH_4)_2SO_4$-K_2SO_4 crystals [32]. In the study, the P_s value for pure AS reaches its maximum (0.6 $\mu C/cm^2$) at ca. 2 K below T_c and continuously decreases until the sign change at ca. 85 K. It should be emphasized that 4 % K-substitution reduces the maximal P_s value of ca. 25 %. The K^+ ion is known to preferentially substitute the NH_4^+(II) [17]. When the K-atom percentage equals 57 % the P_s emerge at ca. 140 K to reach the plateau of 0.23 $\mu C/cm^2$ at lower temperatures [32]. Our earlier studies [39] have shown that the distortion of the SO_4^{2-} from ideal tetrahedron is much lower than the one indicated by the neutron diffraction study [12]. Therefore, the P_s remaining after the total NH_4^+(II) substitution can be ascribed solely to the contribution of the distorted NH_4^+(I). According to the observed P_s vs T dependence the NH_4^+(II) contribution should be of the opposite sign to that of the NH_4^+(I) [32]. Such an assumption is in line with our observation that the main rotation axis of the NH_4^+(II) emerges along the N2−H24 bond and points towards [00$\bar{1}$]. Moreover, the appearance of P_s maximum just after the PT could be induced by the unsuppressed hindered rotations of the NH_4^+(II), which would temporarily cancel the negative contribution to P_s. However, the presented model is incomplete, because the dipole moment values, estimated for distorted cations, are too small to fit the experimental predictions [15,20]. The 'lattice polarization' based on the relative shifts of ions seems to be an improper explanation of the missing contribution. Considering the polar axis, both cations are displaced in opposite directions. Both shifts out of the **ab** plane are small and almost T-independent [39]. Ultimately, such a simple model of the 'lattice polarization' does not explain the substantial reduction of P_s caused by a small substitution of the NH_4^+ with the K^+ ion of a similar size and the same charge. The recently discovered dynamic charge relocation between AS ions [61] seems to better describe the P_s thermal evolution. The charge relocation occurs during the coherent lattice motion, in which main contributions are connected with SO_4^{2-} and NH_4^+(II) (labeled as NH_4^+(1) in [61]). Such charge relocation should be highly temperature-dependent as well as particularly vulnerable to the destabilization of multipole interactions caused by the cation substitution. Further calculations based on the *Modern theory of polarization* [62] would be essential for the verification of the proposed hypothesis of the P_s origin.

4. Conclusions

The considered phase transition mechanism in AS is of a mixed displacive − order-disorder nature, where the anion precession disrupts the balance between two minima in the double-well potential corresponding to the PE and FE orientations of the NH_4^+(I). According to the PT description, it should be classified as the one of the pseudo-proper type. The obtained BOMD results indicate that in the coupled oscillator-relaxator model of PT [14], the role of the 'oscillator' should not be ascribed to NH_4^+(I)-SO_4^{2-} translations. Instead, the relaxation of NH_4^+(I) hindered rotations is connected with the coupling between NH_4^+(I) librations and SO_4^{2-} ν_2 modes, which is induced by the anion precession (see sections 3.3 and 3.4). In such structural transformation, the T_c would not be affected by the deuteration of cations as was found experimentally by Hoshino et al [60]. The inverse barocaloric effect reported for AS [8] is caused by the endothermic stabilization process of the reverse H-bond system reorganization induced by the applied hydrostatic pressure in the vicinity of T_c. The spontaneous polarization in AS is the secondary effect caused by the structural transformation to the polar symmetry. The substantial part of the P_s is probably connected to the charge relocation observed in the ultrafast X-ray diffraction experiment [61]. However, the contribution of both distorted NH_4^+ cations cannot be neglected in the P_s analysis.

The results of our ion dynamics analysis have indicated that the description of the PE phase, which assumed the disorder of all types of ions [8,25,38], is false. In agreement with the structural analysis, our calculations have shown that SO_4^{2-} ions are not disordered up to 298 K (i.e. 75 K above the T_c). Our BOMD simulations for the first time enabled the comprehensive description of NH_4^+(I) and NH_4^+(II) motions which should be classified as the dynamic disorder. The tetrahedral reorientations, can be considered as the Markovian process [63] and do not freeze during the PT. The residence time for both cations are similar at RT (10^{-11} s) and start to differ from each other with temperature decrease. Because of the detected very short randomization time (10^{-13}-10^{-14} s), the reorientations as well as the hindered rotations, cannot be recognized by neutron and X-ray diffraction experiments even at low temperatures. The pre-optimized simulations (MDaOPT) of supercell systems in the P1 symmetry allowed us to reproduce geometrical features of experimental AS crystal structures in both phases. The systems containing only one unit cell as well as the calculations without preceding optimization (MD) do not replicate the experimentally observed H-bond system of AS at any studied temperature.

The presented computational approach provides the description of complicated ion dynamics in the AS crystals with a complex H-bond system. Our investigation scheme should be useful for the studies of PT mechanisms in other H-bonded ferroelectrics and barocaloric materials, e.g. such as plastic crystals [64].

Accession Codes

CSD 2008183–2008184 contain the supplementary crystallographic data for this paper. These data can be obtained free of charge from FIZ Karlsruhe via www.ccdc.cam.ac.uk/stuctures.

Author Contributions

The manuscript was written through contributions of all authors. All authors have given approval to the final version of the manuscript.

Declaration of Competing Interest

The authors declare that they have no known competing financial interests or personal relationships that could have appeared to influence the work reported in this paper.

Acknowledgments

The authors would like to thank Dr. M. Boczar, Dr. A. Krawczuk and Dr. M. Gryl for fruitful discussions. Presented computations were performed using PL-Grid Infrastructure and resources provided by ACC Cyfronet AGH (Academic Computer Centre Cyfronet, University of Science and Technology, Cracow). The publication was funded by the Priority Research Area Anthropocene under the program “Excellence Initiative – Research University” at the Jagiellonian University in Krakow. This research was supported by the National Science Centre Poland, grant number 2018/29/N/ST3/00703.

Supplementary materials

Supplementary material associated with this article can be found, in the online version, at doi:10.1016/j.actamat.2021.116782.

References

[1] X. Moya, S. Kar-Narayan, N.D. Mathur, Caloric materials near ferroic phase transitions, Nat. Mater. 13 (2014) 439–450.
[2] J.M. Bermúdez-García, M. Sánchez-Andújar, M.A. Señarís-Rodríguez, A New Playground for Organic–Inorganic Hybrids: Barocaloric Materials for Pressure-Induced Solid-State Cooling, J. Phys. Chem. Lett. 8 (2017) 4419–4423.
[3] Y. Liu, J.F. Scott, B. Dkhil, Some strategies for improving caloric responses with ferroelectrics, APL Materials 4 (2016) 064109.
[4] B. Yu, M. Liu, P.W. Egolf, A. Kitanovski, A review of magnetic refrigerator and heat pump prototypes built before the year 2010, Int. J. Refrig. 33 (2010) 1029–1060.
[5] T. Zhang, X.-S. Qian, H. Gu, Y. Hou, Q.M. Zhang, An electrocaloric refrigerator with direct solid to solid regeneration, Appl. Phys. Lett. 110 (2017) 243503.
[6] R. Ma, Z. Zhang, K. Tong, D. Huber, R. Kornbluh, Y.S. Ju, Q. Pei, Highly efficient electrocaloric cooling with electrostatic actuation, Science 357 (2017) 1130–1134.
[7] E. Defay, R. Faye, G. Despesse, H. Strozyk, D. Sette, S. Crossley, X. Moya, N.D. Mathur, Enhanced electrocaloric efficiency via energy recovery, Nat. Commun. 9 (2018) 1827.
[8] P. Lloveras, E. Stern-Taulats, M. Barrio, J.-Ll. Tamarit, S. Crossley, W. Li, V. Pomjakushin, A. Planes, Ll. Mañosa, N.D. Mathur, X Moya, Giant barocaloric effects at low pressure in ferrielectric ammonium sulphate, Nat. Commun. 6 (2015) 8801.
[9] S. Crossley, W. Li, X. Moya, N.D. Mathur, Large electrocaloric effects in single-crystal ammonium sulfate, Phil. Trans. R. Soc. A 374 (2016) 20150313.
[10] M.E. Lines, A.M. Glass, Principles and Applications of Ferroelectrics and Related Materials, Oxford University Press, Oxford, 1979.
[11] B.T. Matthias, J.P. Remeika, Ferroelectricity in Ammonium Sulfate, Phys. Rev. 103 (1956) 262.
[12] E.O. Schlemper, W.C. Hamilton, Neutron Diffraction Study of the Structures of Ferroelectric and Paraelectric Ammonium Sulfate, J. Chem. Phys. 44 (1966) 4498–4509.
[13] B.H. Torrie, C.C. Lin, O.S. Binbrek, A. Anderson, Raman and Infrared Studies of the Ferroelectric Transition in Ammonium Sulfate, J. Phys. Chem. Solids 33 (1972) 697–709.
[14] J. Petzelt, J. Grigas, I. Mayerova, Far Infrared Properties of the Pseudoproper Ammonium Sulfate, Ferroelectrics 6 (1973) 225–234.
[15] Y.S. Jain, H.D. Bist, A Point Charge Model for the Ferroelectric Transition in Ammonium Sulfate, Phys. Status Solidi B 62 (1974) 295–300.
[16] P.K. Bajpai, Y.S. Jain, The phase transition in ammonium sulfate: dynamics of deuterated NH_4^+ ions and the heat of transition, J. Phys. C: Solid State Phys. 20 (1987) 387–393.
[17] D. De Sousa Meneses, G. Hauret, P. Simon, F. Brehat, B. Wyncke, Phase-transition mechanism in $(NH_4)_2SO_4$, Phys. Rev. B: Condens. Matter Mater. Phys. 51 (1995) 2669–2677.
[18] Z. Iqbal, C.W. Christoe, Raman scattering study of ferroelectric phase transition in ammonium sulfate, Solid State Commun 18 (1976) 269–273.
[19] H. Yurtseven, H. Karacali, A. Kiraci, Calculation of the damping constant and activation energy for Raman modes in $(NH_4)_2SO_4$, Int. J. Mod. Phys. B 25 (2011) 2063–2080.
[20] D.E. O'Reilly, T. Tsang, Deuteron Magnetic Resonance and Proton Relaxation Times in Ferroelectric Ammonium Sulfate, J. Chem. Phys. 46 (1967) 1291–1300.
[21] T.J. Nordland, D.E. O'Reilly, E.M. Peterson, Ferroelectric mode in ammonium sulfate, J. Chem. Phys. 64 (1976) 1838–1841.
[22] N. Shibata, R. Abe, I. Suzuki, ESR Study of NH_3^+ and SeO_3^- Radicals in $(NH_4)_2SO_4$, J. Phys. Soc. Jpn. 41 (1976) 2011–2019.
[23] R. Abe, N. Shibata, A Microscopic Model for the Ferroelectric Phase Transition in $(NH_4)_2SO_4$, J. Phys. Soc. Jpn. 43 (1977) 1308–1313.
[24] A. Onodera, Y. Sugata, Y. Shiozaki, Ferrielectric dielectric behaviour and the nature of phase transition of ammonium sulfate, Solid State Commun 27 (1978) 243–245.
[25] G. Kozlov, S. Lebedev, A. Volkov, J. Petzelt, B. Wyncke, F. Bréhat, Dielectric dispersion of $(NH_4)_2SO_4$ in the near-millimetre and far-infrared range: Manifestations of disorder, J. Phys. C: Solid State Phys. 21 (1988) 4883–4894.
[26] A. Onodera, H. Fujishita, Y. Shiozaki, X-ray diffraction study of sub-lattice order parameters in ferrielectric ammonium sulphate, Solid. State. Commun. 27 (1978) 463–465.
[27] K. Hasebe, Studies of the crystal structure of ammonium sulfate in connection with its ferroelectric phase transition, J. Phys. Soc. Japan 50 (1981) 1266–1274.
[28] W.C. Hamilton, Comment on the Order–Disorder Transition in Ferroelectric Ammonium Sulfate, J. Chem. Phys. 50 (1969) 2275.
[29] U. Dahlborg, K.E. Larsson, E. Pirkmajer, Rotational motions in solids. The ferroelectric transition in $(NH_4)_2SO_4$, Physica 49 (1970) 1–25.
[30] P.S. Goyal, R. Chakravarthy, B.A. Dasannacharya, C.J. Carlile, Reorientations of NH_4^+ Ions in the Ferroelectric Phase of $(NH_4)_2SO_4$, Phys. Status Solidi A 18 (1990) 425–430.
[31] H.G. Unruh, The spontaneous polarization of $(NH_4)_2SO_4$, Solid. State. Commun. 8 (1970) 1951–1954.
[32] A. Sawada, S. Ohya, Y. Ishibashi, Y. Takagi, Ferroelectric Phase-Transition in $(NH_4)_2SO_4$-K_2SO_4 Mixed Crystals, J. Phys. Soc. Japan 38 (1975) 1408–1414.
[33] S. Sawada, T. Yamaguchi, N. Shibayama, Ferrielectricity in $(NH_4)_2SO_4$, $(NH_4)_2BeF_4$ and K_2SeO_4, J. Phys. Soc. Japan 48 (1980) 1395–1396.
[34] A. Sawada, Y. Takagi, Y. Ishibashi, The Origin of the Ferroelectric Phase Transition in Ammonium Sulfate, J. Phys. Soc. Japan 34 (1973) 748–754.
[35] K. Hasebe, Phase transition of ammonium sulfate, J. Phys. Soc. Japan. 50 (1981) 2660–2665.
[36] A. Onodera, O. Cynshi, Y. Shiozaki, Landau theory of the ferrielectric phase transition with two order parameters, J. Phys. C: Solid State Phys. 18 (1985) 2831–2841.

[37] Y.S. Jain, P.K. Bajpai, R. Bhattacharjee, D. Chowdhury, Phase transition and temperature dependence of the molecular distortion of ions in ammonium sulphate, J. Phys. C: Solid State Phys. 19 (1986) 3789–3796.
[38] D. De Sousa Meneses, Phenomenological Landau theory of the $(NH_4)_2SO_4$ para-ferroelectric phase transition, Solid. State. Commun. 96 (1995) 5–9.
[39] L.M. Malec, M. Gryl, K.M. Stadnicka, Unmasking the Mechanism of Structural Para- to Ferroelectric Phase Transition in $(NH_4)_2SO_4$, Inorg. Chem. 57 (2018) 4340–4351.
[40] G. Cametti, T. Armbruster, J. Hermann, S. Churakov, Crystal structure and phase transition in noelbensonite: a multi-methodological study, Phys. Chem. Minerals 44 (2017) 485–496.
[41] P.C. Aeberhard, K. Refson, W.I.F. David, Molecular dynamics investigation of the disordered crystal structure of hexagonal $LiBH_4$, Phys. Chem. Chem. Phys. 15 (2013) 8081–8087.
[42] M.A. Carignano, A. Kachmar, J. Hutter, Thermal effects on $CH_3NH_3PbI_3$ perovskite from ab initio molecular dynamics simulations, J. Phys. Chem. C 119 (2015) 8991–8997.
[43] J. Even, M. Carignano, C. Katan, Molecular disorder and translation/rotation coupling in the plastic crystal phase of hybrid perovskites, Nanoscale 8 (2016) 6222–6236.
[44] J. Hutter, M. Iannuzzi, F. Schiffmann, J. VandeVondele, CP2K: atomistic simulations of condensed matter systems, WIREs Comput. Mol. Sci. 4 (2014) 15–25.
[45] J. VandeVondele, M. Krack, F. Mohamed, M. Parrinello, T. Chassaing, J. Hutter, QUICKSTEP: fast and accurate density functional calculations using a mixed Gaussian and plane waves approach, Comput. Phys. Commun. 167 (2005) 103–128.
[46] A.D. Becke, Density–functional thermochemistry. III. The role of exact exchange, J. Chem. Phys. 98 (1993) 5648–5652.
[47] C. Lee, W. Yang, R.G. Parr, Development of the Colle–Salvetti correlation – energy formula into a functional of the electron density, Phys. Rev. B 37 (1988) 785–789.
[48] S. Grimme, J. Antony, S. Ehrlich, H. Krieg, A Consistent and Accurate Ab Initio Parametrization of Density Functional Dispersion Correction (DFT-D) for the 94 Elements H-Pu, J. Chem. Phys. 132 (2010) 154104.
[49] G. Lippert, J. Hutter, M. Parrinello, A hybrid Gaussian and plane wave density functional scheme, Mol. Phys. 92 (1997) 477–488.
[50] S. Goedecker, K. Maschke, Transferability of pseudopotentials, Phys. Rev. A 45 (1992) 88–93.
[51] S. Nose, An extension of the canonical ensemble molecular dynamics method, Mol. Phys. 57 (1986) 187–191.
[52] W.G. Hoover, Canonical dynamics: Equilibrium phase–space distributions, Phys. Rev. A 31 (1985) 1695–1697.
[53] W. Humphrey, A. Dalke, K. Schulten, VMD: visual molecular dynamics, J. Mol. Graph. 14 (1996) 33–38.
[54] H. Forbert, A. Kohlmeyer, Fourier., version 1.1, Rurh Universitat Bochum, Bochum, Germany, 2002–2008.
[55] G.A. Jeffrey, An Introduction to Hydrogen Bonding, Oxford University Press, Oxford, 1997.
[56] P. Muller, R. Herbst-Irmer, A.L. Spek, T.R. Schneider, M.R. Sawaya, Crystal Structure Refinement A Crystallographer's Guide to SHELXL, Oxford University Press, Oxford, 2006.
[57] M. Thomas, M. Brehm, R. Fligg, P. Vohringer, B. Kirchner, Computing vibrational spectra from ab initio molecular dynamics, Phys. Chem. Chem. Phys. 15 (2013) 6608–6622.
[58] K. Nakamoto, Infrared and Raman Spectra of Inorganic and Coordination Compounds, Part A: Theory and Applications in Inorganic Chemistry, 6th Ed., John Wiley & Sons, New Jersey, 2009.
[59] R.L. Carter, Single-crystal Raman spectra of paraelectric $(NH_4)_2SO_4$, Spectrochim. Acta, Part A 32 (1976) 575–579.
[60] S. Hoshino, K. Vedam, Y. Okaya, R. Pepinsky, Dielectric and Thermal Study of (NH4)2SO4 and (NH4)2BeF4 Transitions, Phys. Rev. 112 (1958) 405–412.
[61] C. Hauf, A.-A. Hernandez Salvador, M. Holtz, M. Woerner, T. Elsaesser, Soft-mode driven polarity reversal in ferroelectrics mapped by ultrafast x-ray diffraction, Struct. Dyn. 5 (2018) 024501.
[62] R. Resta, Macroscopic polarization in crystalline dielectrics: the geometric phase approach, Rev. Modern Phys. 66 (1994) 899–915.
[63] C. Gardiner, Stochastic Methods: A Handbook for the Natural and Social Sciences, 4th Ed., Springer-Verlag, Berlin, Heidelberg, 2009.
[64] A. Aznar, P. Lloveras, M. Barrio, P. Negrier, A. Planes, L. Mañosa, N.D. Mathur, X. Moya, J.-L. Tamarit, Reversible and irreversible colossal barocaloric effects in plastic crystals, J. Mater. Chem. A 8 (2020) 639–647.